Electronic Supplementary Information

Multimetallic layered double hydroxides as efficient and durable oxygen evolution catalysts for anion exchange membrane water electrolysis at high current densities

Yaowen Xu,[‡,a,b] Kaiyang Xu,[‡,b] Hao Tan,[a,b] Haoliang Huang,[b] Fei Lin,[b] Chenyue Zhang,[b] Jingwei Wang,[b] Run Ran,[b] Jinfeng Zeng,[b] Zhipeng Yu,[c] Sitaramanjaneya Mouli Thalluri,[c] Lijian Meng,[d] Dehua Xiong,*[a] and Lifeng Liu*[b]

[a] State Key Laboratory of Silicate Materials for Architectures, Wuhan University of Technology, Wuhan 430070, P. R. China.

[b] Songshan Lake Materials Laboratory (SLAB), Dongguan 523808, P. R. China.

[c] International Iberian Nanotechnology Laboratory (INL), Avenida Mestre Jose Veiga, 4715-330 Braga, Portugal.

[d] Centre of Innovation in Engineering and Industrial Technology, Instituto Superior de Engenharia do Porto, Instituto Politecnico do Porto, 4249-015 Porto, Portugal.

[‡] Y.W.X. and K.J.X. contributed equally to this work.

* To whom correspondence should be made (D. H. X and L. L.).

E-mail: xiongdehua@whut.edu.cn (D. H. Xiong); liu.lifeng@sslab.org.cn (L. Liu)

Supplementary Figures

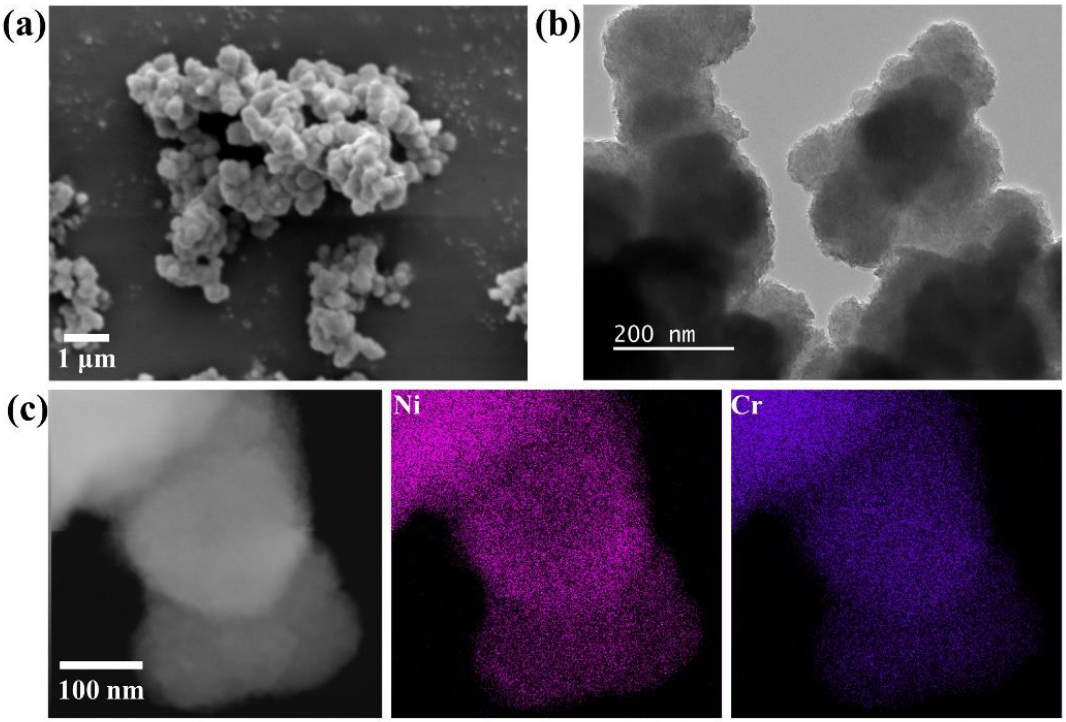

Fig. S1 (a) SEM image and (b) TEM image of NiCr LDHs. (c) EDS elemental maps of Ni and Cr.

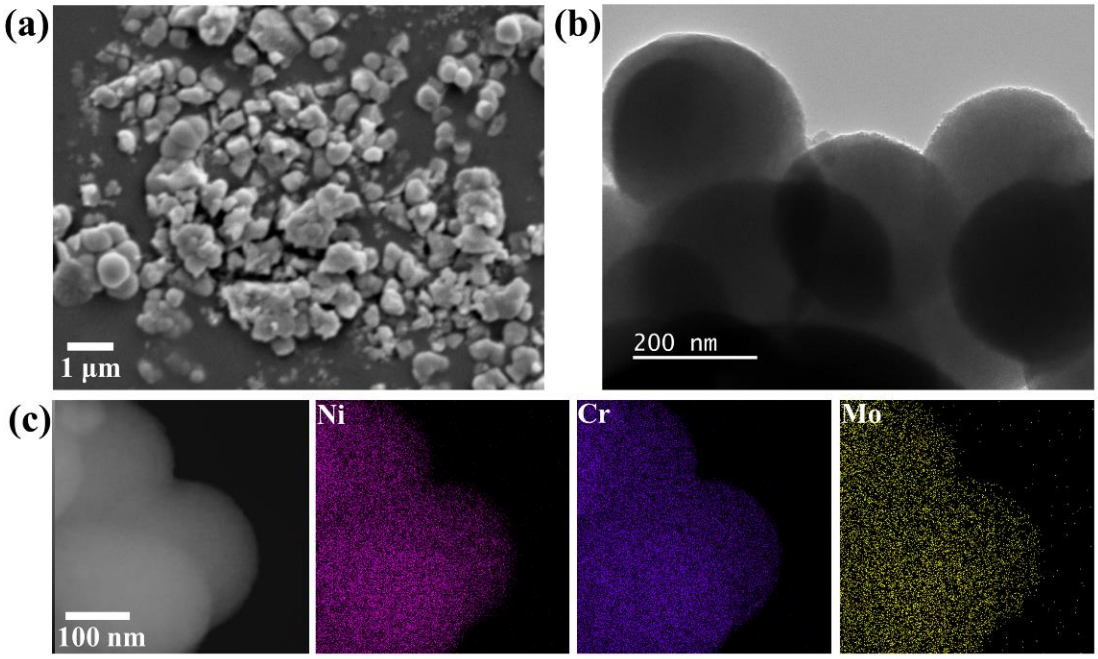

Fig. S2 (a) SEM image and (b) TEM image of NiCrMo LDHs. (c) EDS elemental maps of Ni, Cr, and Mo.

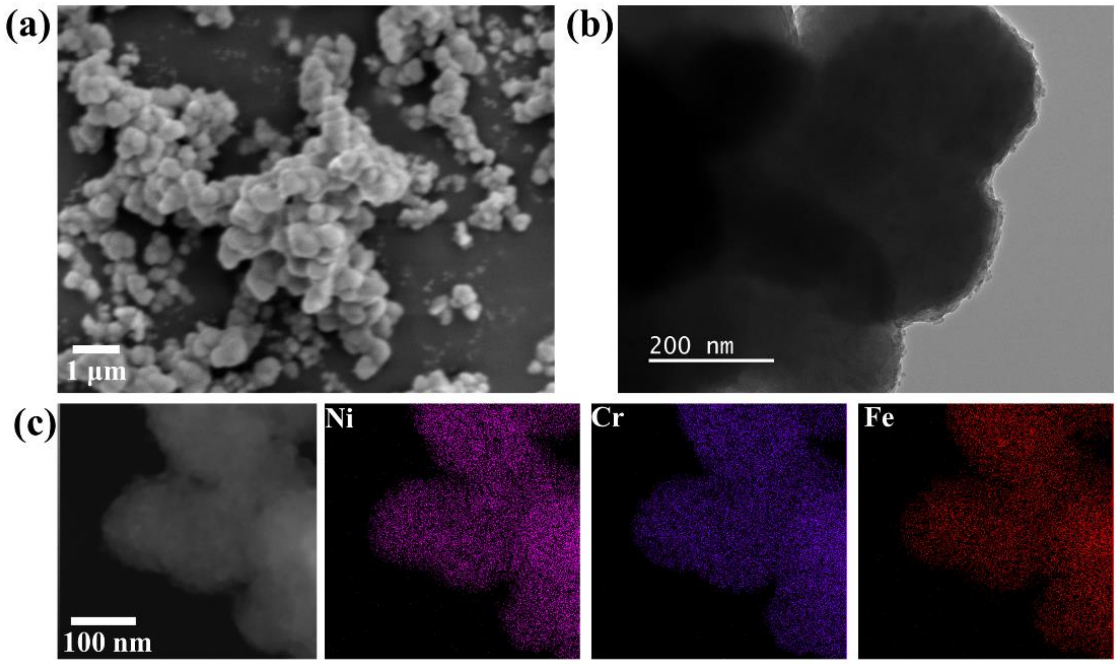

Fig. S3 (a) SEM image and (b) TEM image of NiCrFe LDHs. (c) EDS elemental maps of Ni, Cr, and Fe.

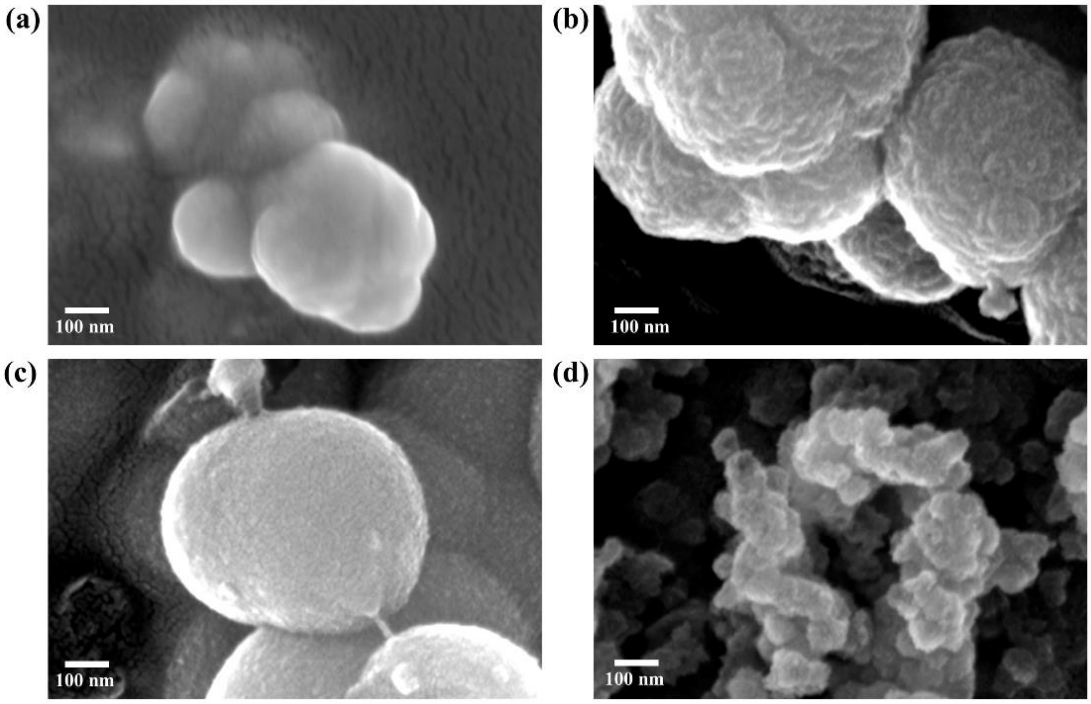

Fig. S4 High-magnification SEM images of (a) NiCr, (b) NiCrMo, (c) NiCrFe, and (d) NiCrFeMo LDHs.

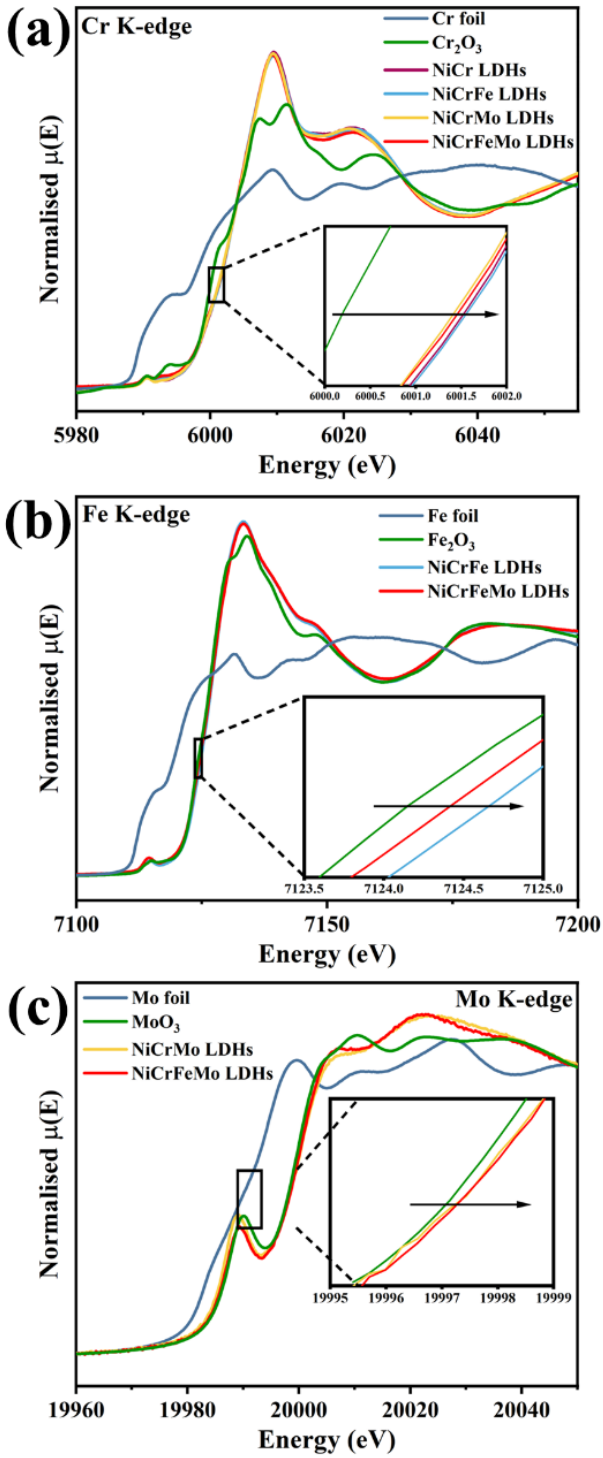

Fig. S5 XANES spectra of different LDHs acquired at (a) Cr K-edge, (b) Fe K-edge, and (c) Mo K-edge

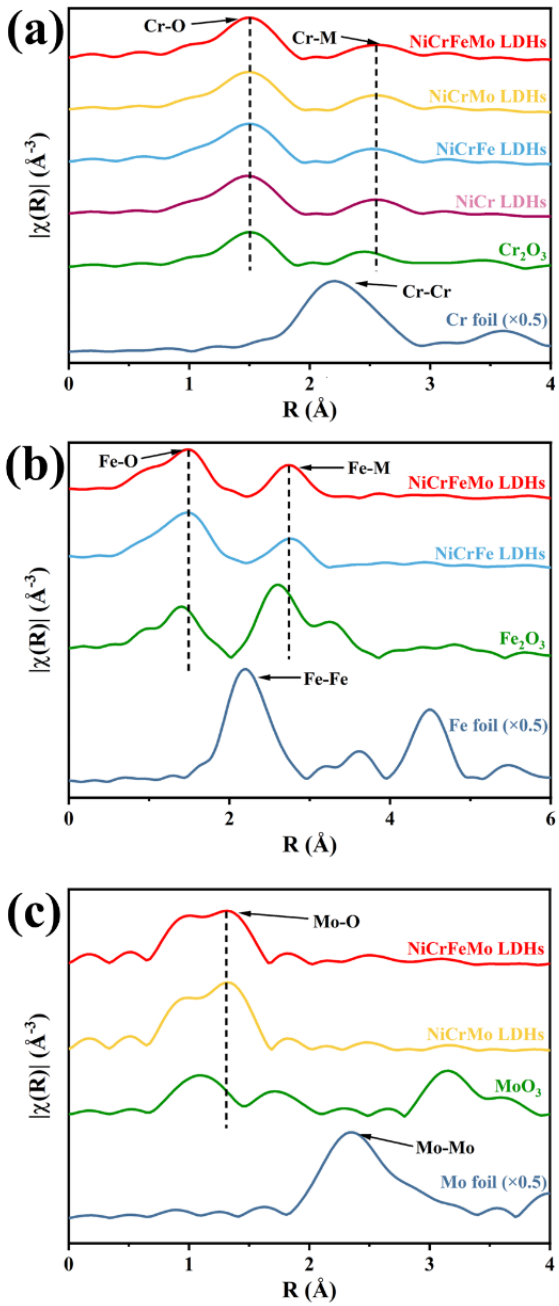

Fig. S6 FT-EXAFS spectra of different LDHs acquired at (a) Cr K-edge, (b) Fe-K edge, and (c) Mo K-edge.

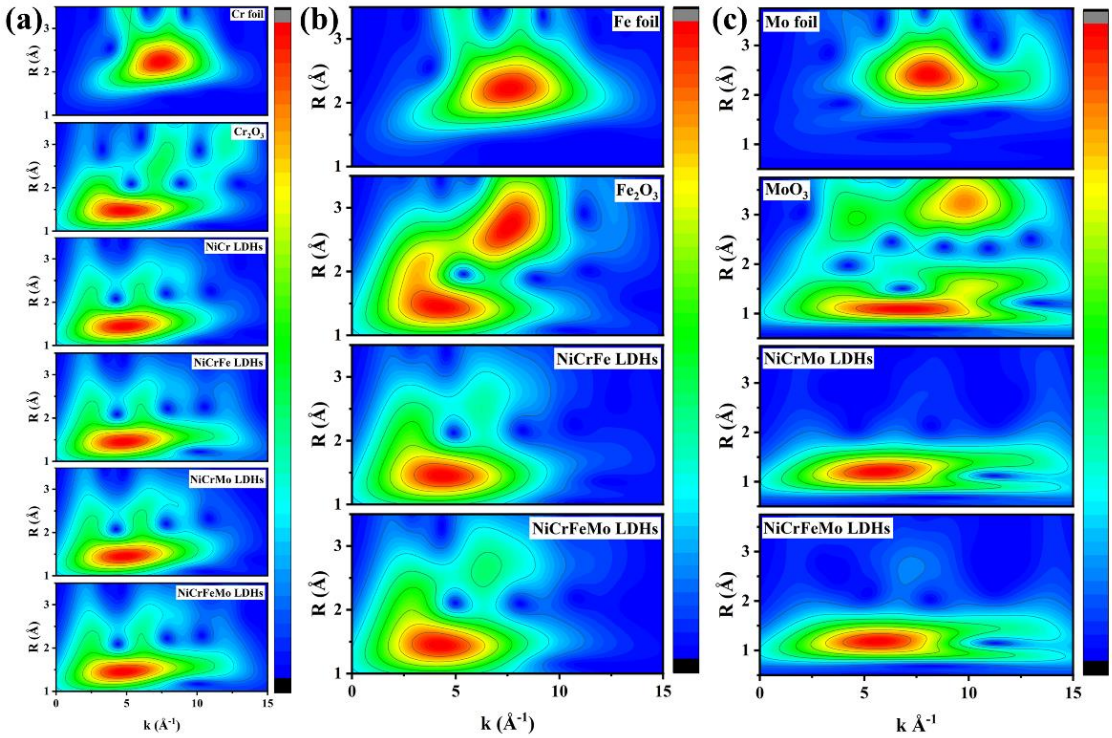

Fig. S7 Wavelet transform contour maps of the (a) Cr K-edge, (b) Fe K-edge and (c) Mo K-edge EXAFS for different LDHs catalysts.

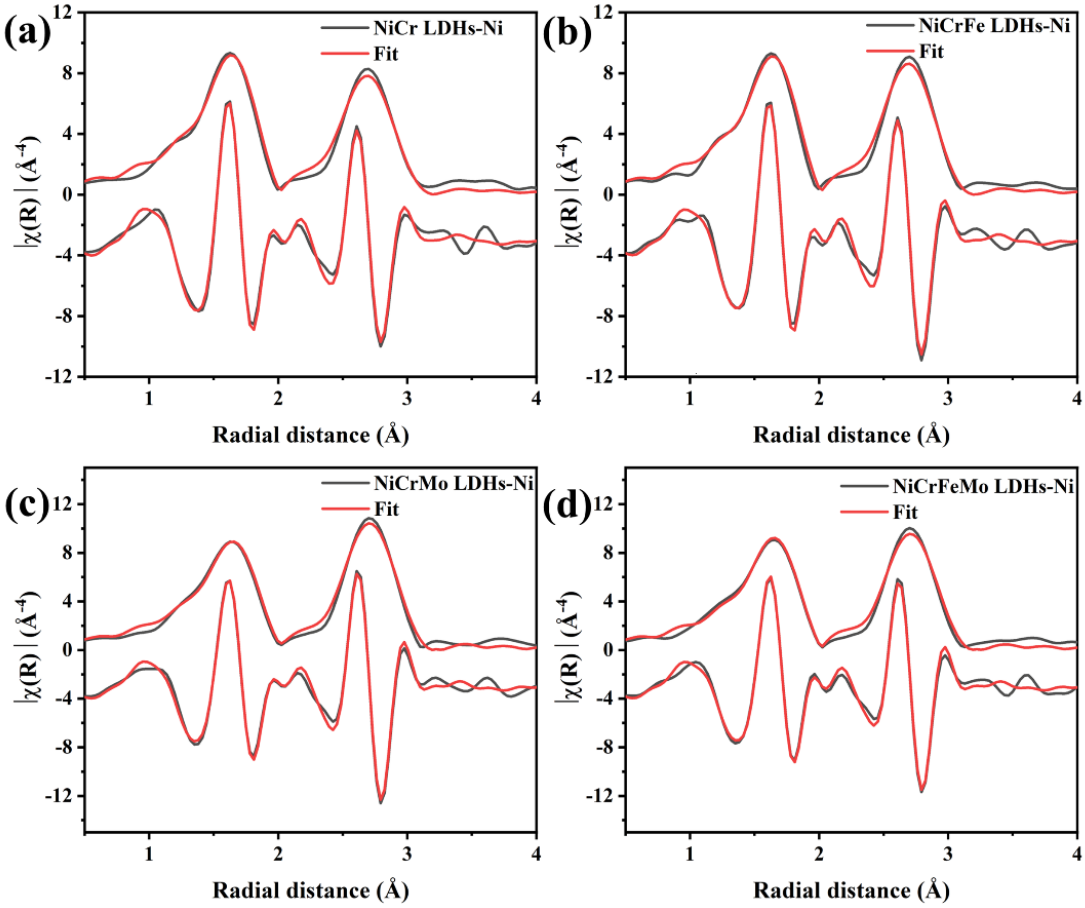

Fig. S8 Fits of EXAFS spectra of Ni–O bond of the (a) NiCr, (b) NiCrFe, (c) NiCrMo and (d) NiCrFeMo LDHs. The fitting curves are presented in the form of amplitude as a function of the real part of R space. The obtained structural parameters are listed in **Table S2**, and the real part of the Fourier transform is on purpose shifted downwards for clarity.

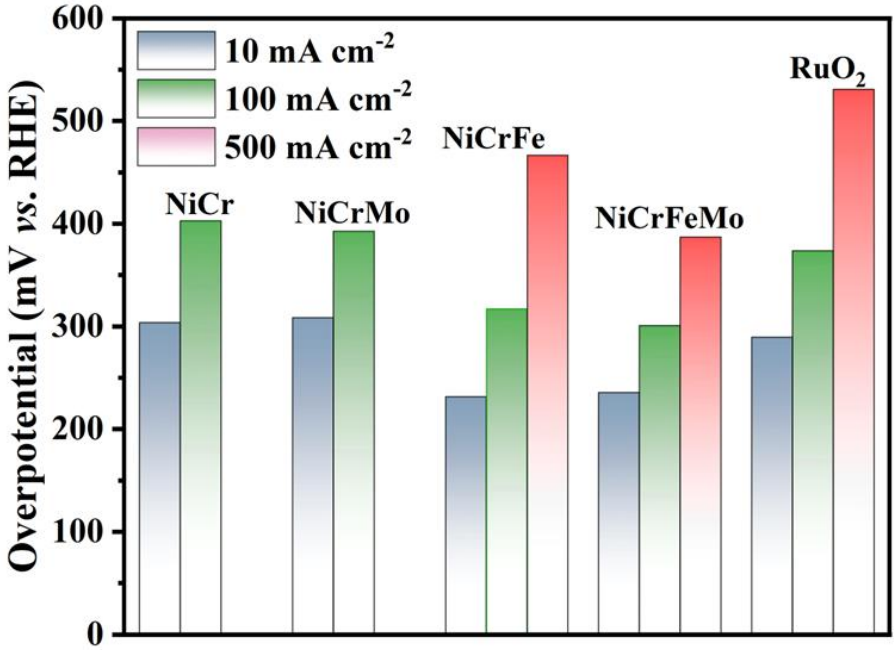

Fig. S9 The overpotentials of various catalysts at different current densities.

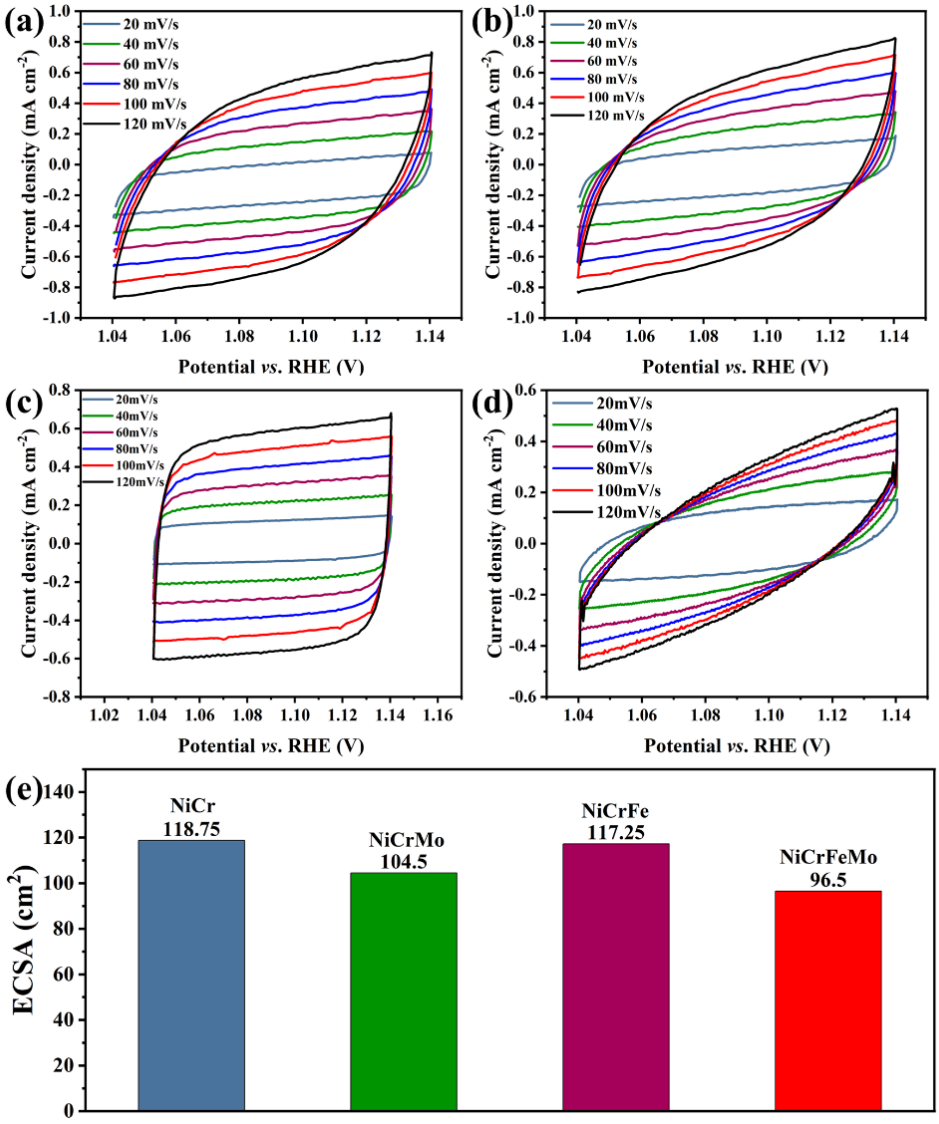

Fig. S10 Electrochemical CV curves of (a) NiCr LDHs, (b) NiCrMo LDHs, (c) NiCrFe LDHs, and (d) NiCrFeMo LDHs, recorded at different scan rates of 20, 40, 60, 80, 100, and 120 mV s^{-1}. (e) ECSA values of LDHs.

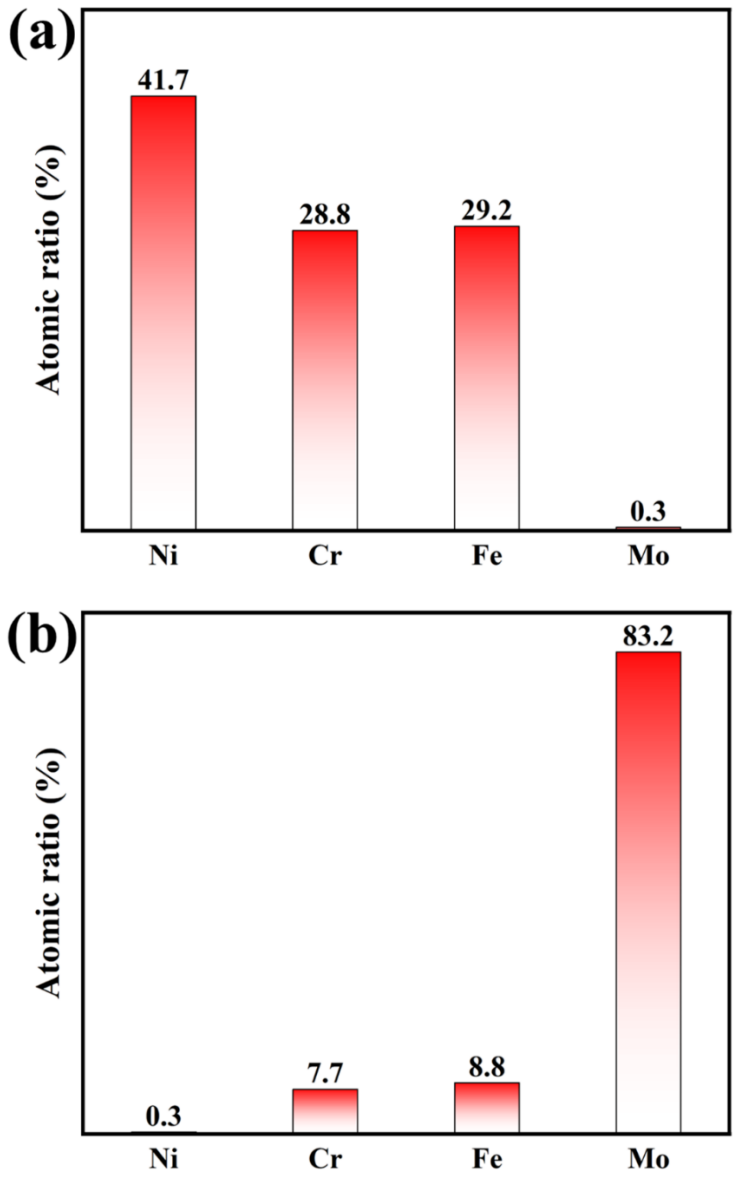

Fig. S11 (a) The metal content changes in the NiCrFeMo catalysts after the stability test at 500 mA cm^{-2} for 60 hours, measured by ICP-MS. (b) The metal content in the electrolyte after the stability test.

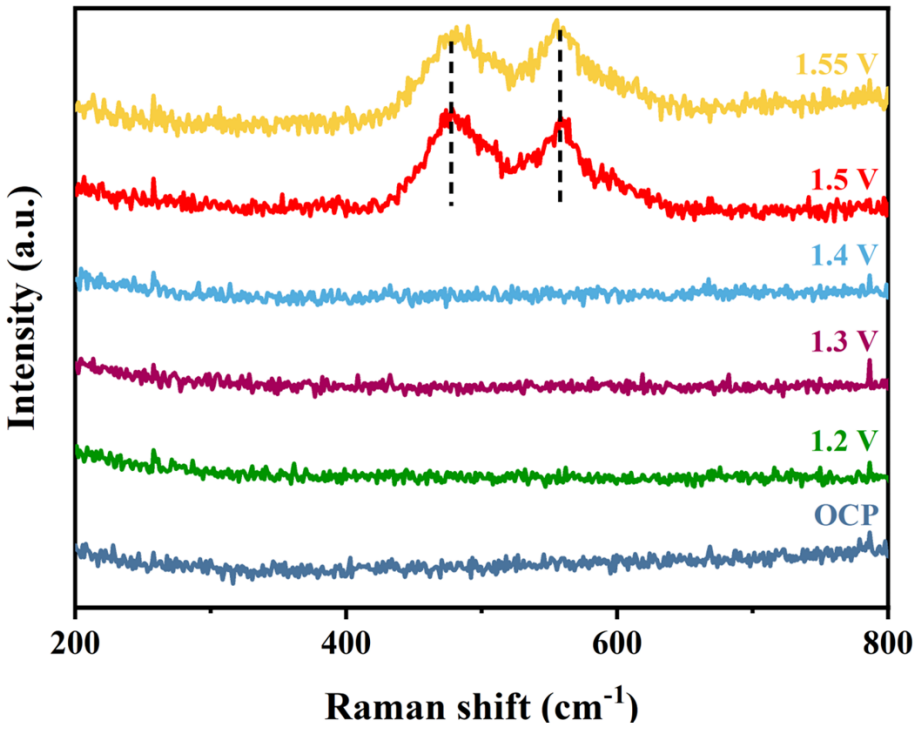

Fig. S12 In-situ Raman spectra of NiCrFeMo LDH electrocatalysts collected at different applied potentials ranging from OCP to 1.55 V vs. RHE.

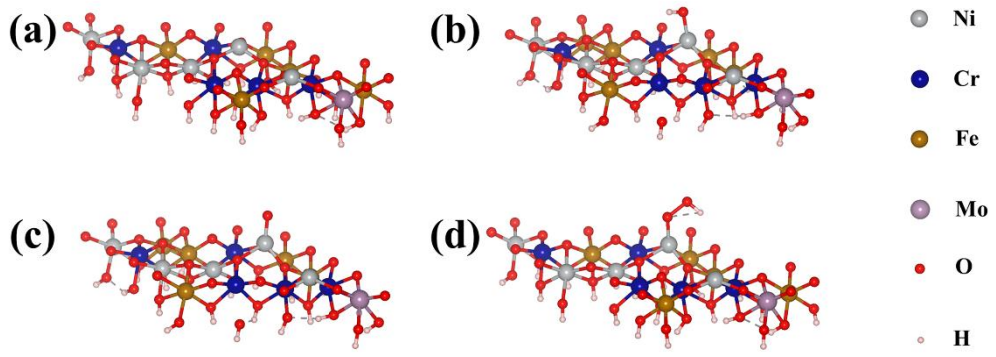

Fig. S13 Models with Ni as the active site used to illustrate the adsorbate evolving mechanism on the NiCrFeMoOOH surface adsorbed with (a) *, (b) *OH, (c) *O, and (d) *OOH.

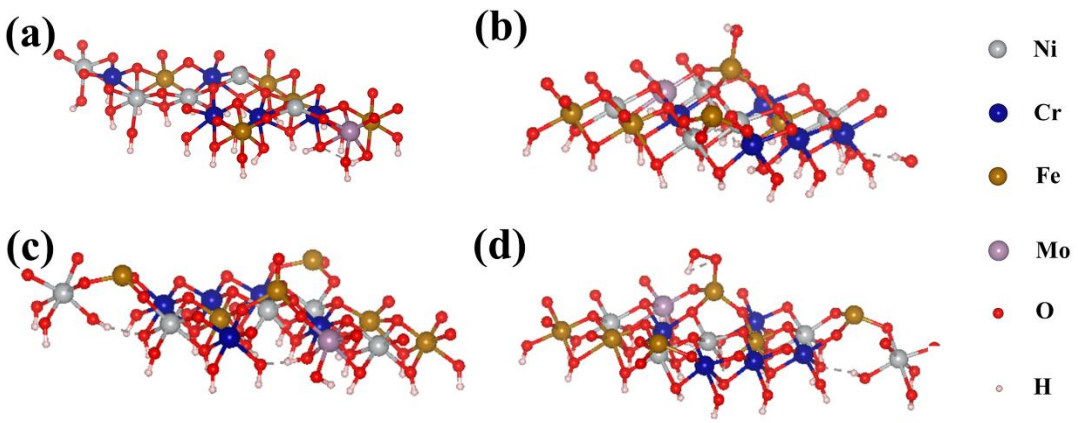

Fig. S14 Models with Fe as the active site used to illustrate the adsorbate evolving mechanism on the NiCrFeMoOOH surface adsorbed with (a) *, (b) *OH, (c) *O, and (d) *OOH.

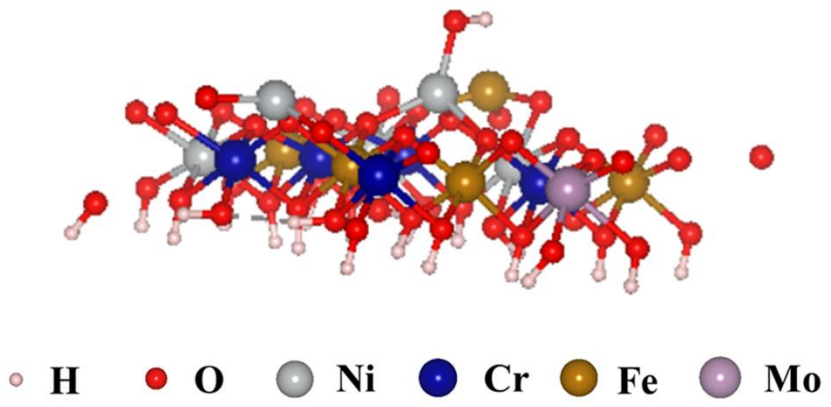

Fig. S15 The model with Cr as the active site on the NiCrFeMoOOH surface adsorbed with *OH. The adsorbed OH species would spontaneously migrate to the Ni site, indicating that Cr is not hydroxyl-philic.

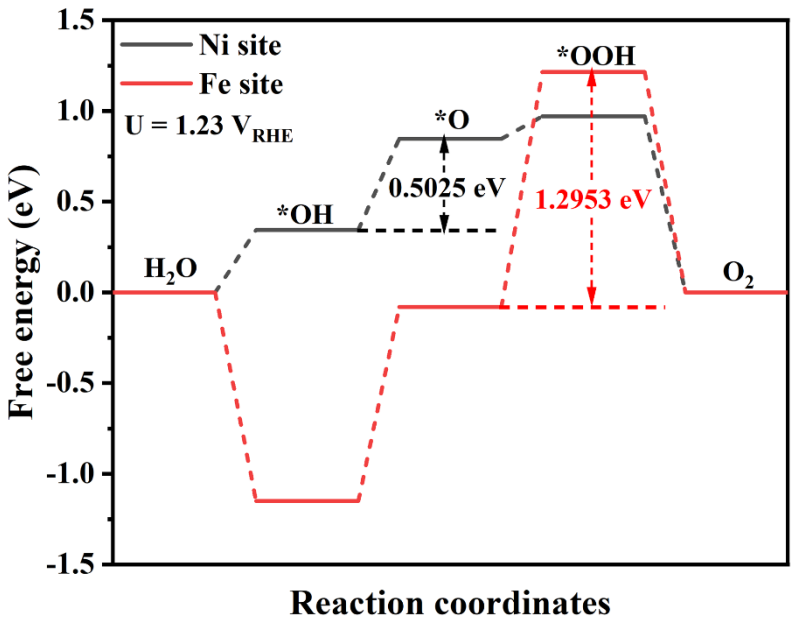

Fig. S16 Gibbs free energy diagrams of NiCrFeMoOOH calculated based on the adsorbate evolving mechanism with Ni and Fe as active sites, respectively.

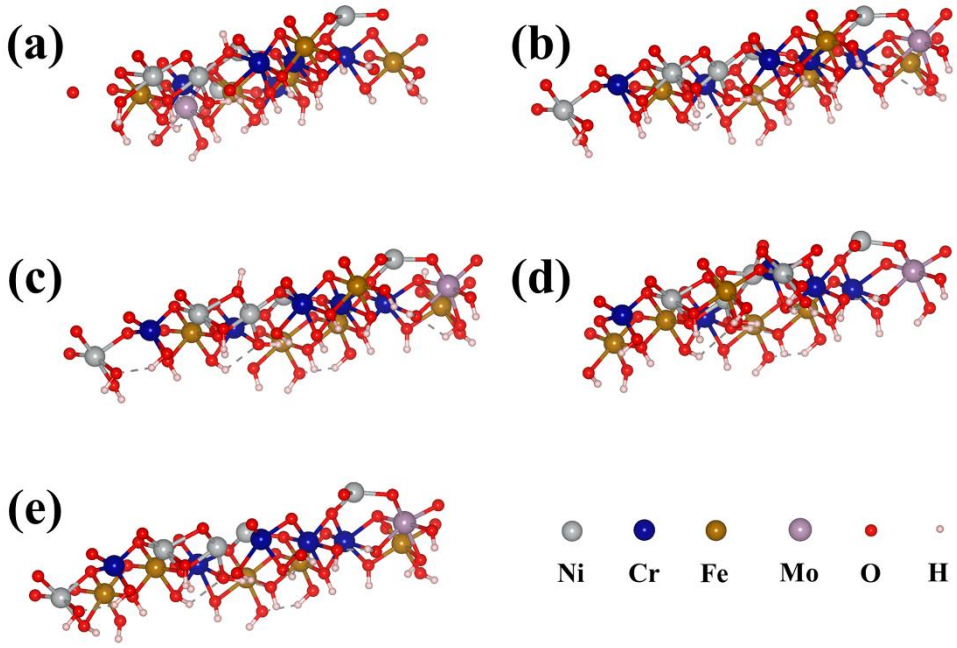

Fig. S17 Models used to illustrate the lattice oxygen mechanism on the NiCrFeMoOOH surface adsorbed with (a) *OH, (b) *O, (c) *OOH, (d) *OO, and (e) V_O.

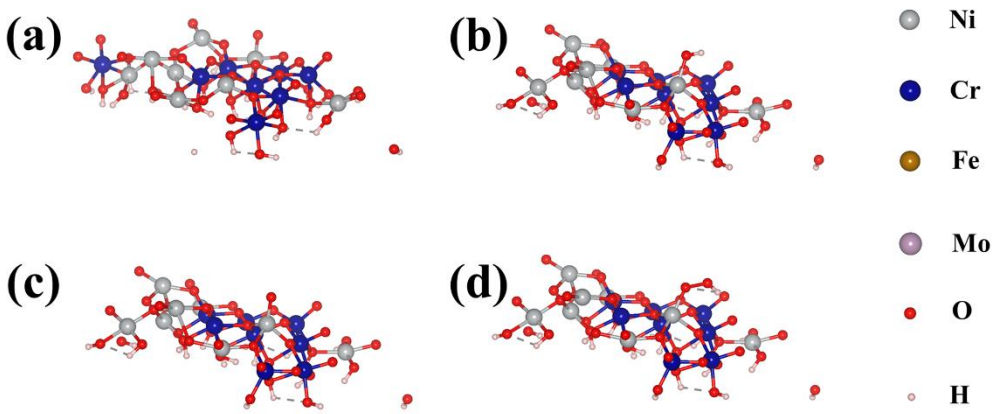

Fig. S18 Models used to illustrate the adsorbate evolving mechanism on the NiCrOOH surface adsorbed with of (a) *, (b) *OH, (c) *O, and (d) *OOH.

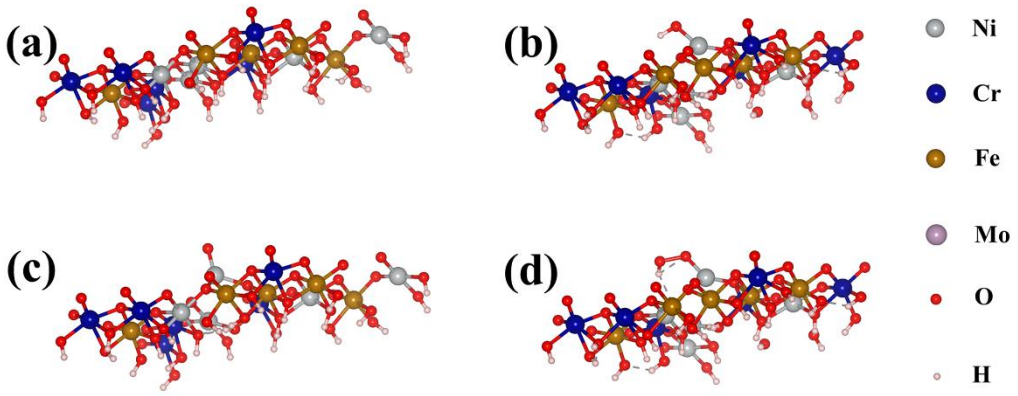

Fig. S19 Models used to illustrate the adsorbate evolving mechanism on the NiCrFeOOH surface adsorbed with (a) *, (b) *OH, (c) *O, and (d) *OOH.

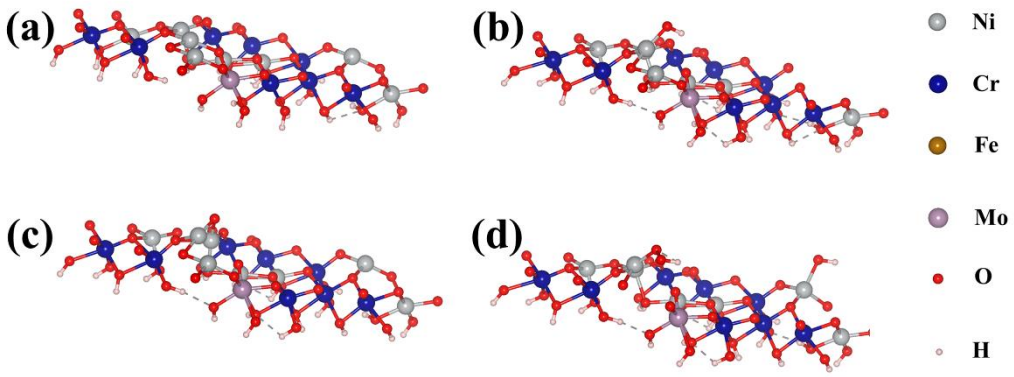

Fig. S20 Models used to illustrate the adsorbate evolving mechanism on the NiCrMoOOH surface adsorbed with (a) *, (b) *OH, (c) *O, and (d) *OOH.

Supplementary Tables:

Table S1. The experimental parameters used in the microwave-assisted hydrothermal synthesis of control catalysts.

Precursors* / Control catalysts	$NiCl_2 \cdot 6H_2O$	$CrCl_3 \cdot 6H_2O$	$FeCl_3 \cdot 6H_2O$	Na_2MoO_4
NiCr LDHs	2 mmol	2 mmol	\	\
NiCrFe LDHs	1 mmol	1 mmol	1 mmol	\
NiCrMo LDHs	1 mmol	1 mmol	\	1 mmol

* The amounts of NH_4F and urea are 10 and 20 mmol, respectively, in all cases. Other experimental conditions are kept the same as those for NiCrFeMo LDHs.

Table S2. Structural parameters of NiCr, NiCrFe, NiCrMo and NiCrFeMo LDHs, obtained from EXAFS fitting shown in **Fig. S8**.[a]

Sample	Scattering path	R (Å)	CN	σ^2 ($\times 10^{-3}$ Å^2)	R factor (%)
NiCr LDHs	Ni–O	2.048 ± 0.005	6.4 ± 0.6	5.7 ± 0.7	0.81
	Ni–Ni	3.050 ± 0.007	7.3 ± 1.1	10.3 ± 1.1	
NiCrFe LDHs	Ni–O	2.048 ± 0.006	6.2 ± 0.6	5.5 ± 0.8	0.65
	Ni–Ni	3.049 ± 0.008	7.3 ± 1.2	9.6 ± 1.2	
NiCrMo LDHs	Ni–O	2.054 ± 0.005	6.5 ± 0.6	6.2 ± 0.8	0.54
	Ni–Ni	3.059 ± 0.006	8.0 ± 1.0	8.8 ± 0.8	
NiCrFeMo LDHs	Ni–O	2.054 ± 0.005	6.3 ± 0.5	5.5 ± 0.7	0.52
	Ni–Ni	3.059 ± 0.006	7.1 ± 0.9	8.6 ± 0.9	

[a] R is the distance between the absorber–scatterer pair, CN represents the coordination number, σ^2 stands for the Debye-Waller (disorder factor), and R factor is a measure of the goodness of fitting.

Table S3. Comparison of the OER performance of NiCrFeMo LDHs with that of other OER electrocatalysts reported recently in the literature.

Electrocatalysts	η_{10} (mV)	Stability	Reference
NiCrFeMo LDHs	**236**	**1000 h @ 500 mA cm^{-2}**	**This work**
FeCoNiMnCr HEA-HEO/CNT	261	240 h @ 100 mA cm^{-2}	Ref. S1
Co-Fe-Ga-Ni-Zn	370	10 h @ 10 mA cm^{-2}	Ref. S2
CoCrFeNiMo-20 Mg HEA	220	24 h @ 100 mA cm^{-2}	Ref. S3
CoCrFeNiAl HEC	240	240 h @ 10 mA cm^{-2}	Ref. S4
$Mg_{0.2}Co_{0.2}Ni_{0.2}Cu_{0.2}Zn_{0.2}O$ HEO	360	25 h @ 10 mA cm^{-2}	Ref. S5
$Fe_{29}Co_{27}Ni_{23}Si_9B_{12}$-HEA-3h	277	50 h @ 100 mA cm^{-2}	Ref. S6
NiFe-LDH/SnS	310	\	Ref. S7
Fe-Cr-Co-Ni-Cu HE-LDHs-Ar-20	330	24 h @ 10 mA cm^{-2}	Ref. S8
MnFeCoNiCu	263	24 h @ 10 mA cm^{-2}	Ref. S9
FeCoNiMo HEA	250	65 h @ 10 mA cm^{-2}	Ref. S10
$CoNiFeCu_{0.1}$@NF	255	80 h @ 20 mA cm^{-2}	Ref. S11
HEO-NS	255	200 h @ 100 mA cm^{-2}	Ref. S12
$La(CrMnFeCo_2Ni)O_3$	325	50 h @ 10 mA cm^{-2}	Ref. S13
FeNiCoCrMn-G	229	36 h @ 100 mA cm^{-2}	Ref. S14
CoNiFeCu (1:1:1:0.5)	292	25 h @ 10 mA cm^{-2}	Ref. S15
$(CoNiMnZnFe)_3O_{3.2}$	336	20 h @ 9 mA cm^{-2}	Ref. S16
$(Cr_{0.2}Mn_{0.2}Fe_{0.2}Co_{0.2}Ni_{0.2})_3O_4$	332	20 h @ 10 mA cm^{-2}	Ref. S17
$(Fe_{0.2}Co_{0.2}Ni_{0.2}Cr_{0.2}Mn_{0.2})_3O_4$	275	60 h @ 10 mA cm^{-2}	Ref. S18
FeCoNiMnMo SPHEA	279	1000 h @ 10 mA cm^{-2}	Ref. S19
$Ni_{SA}Fe_{SA}$-$Ni_{50}Fe$/CNT	227	65 h @ 10 mA cm^{-2}	Ref. S20
NCMH	291	50 h @ 50 mA cm^{-2}	Ref. S21

Table S4 Comparison of the OER performance of NiCrFeMo LDHs with that of other multimetallic LDH catalysts reported recently in the literature.

Electrocatalysts	η_{10} (mV)	Stability	Reference
NiCrFeMo LDHs	**236**	**1000 h @ 500 mA cm^{-2}**	**This work**
NiCoCu LDH	224	10 h @ 10 mA cm^{-2}	*J. Colloid & Interface Sci.*, **2023**, 647, 104–114
NiFeCo LDH/NF	195	170 h @ 10 mA cm^{-2}	*J. Mater. Chem. A*, **2023**, 11, 22941–22950
$Co_{[4.5]}Cu_{[3]}Fe_{[3]}$-LDH/$G_{[10]}$	350	25 h @ 10 mA cm^{-2}	*ACS Appl. Mater. Interfaces*, **2024**, 16, 50846−50858
CoFe@NiFe-200/NF	223	30 h @ 36 mA cm^{-2}	*Appl. Catal. B: Environ.*, **2019**, 253, 131–139
HELDH-MC/NF,	183	48 h @ 250 mA cm^{-2}	*J. Mater. Chem. A*, **2023**, 11, 13697–13707
Fe-Cr-Co-Ni-Cu HE-LDHs-Ar-20	330	16 h @ 10 mA cm^{-2}	*J. Energy Chem.*, **2021**, 60, 121–126
FeCoNi LDH	218	24 h @ 10 mA cm^{-2}	*Chem. Eng. J.*, **2023**, 452, 139686
NiFeV-LDH	287	/	*Adv. Funct. Mater.*, **2021**, 31, 2009743
NiFeMn LDH	258	160 h @ 100 mA cm^{-2}	*Angew. Chem. Int. Ed.*, **2021**, 60, 9699–9705
$Ni_{0.3}Fe_{0.7}$-LDH@NF	184	84 h @ 10 mA cm^{-2}	*Appl. Catal. B: Environ.*, **2023**, ***323***, 122091
Ru/CoFe-LDHs	198	25 h @ 200 mA cm^{-2}	*Nature Commun.*, **2019**, 10, 1711
d-NiFe LDH	170	900 h @ 10 mA cm^{-2}	*Angew. Chem. Int. Ed.*, **2023**, 62, e202217815
Pt-NiFe LDH	198	3000 h @ 1000 mA cm^{-2} (two-electrode system)	*Appl. Catal. B: Environ.*, **2023**, 331, 122683

References:

S1. J. Hu, T. Guo, X. Zhong, J. Li, Y. Mei, C. Zhang, Y. Feng, M. Sun, L. Meng, Z. Wang, B. Huang, L. Zhang and Z. Wang, *Adv. Mater.*, 2024, **36**, 2310918.

S2. L. Sharma, N. K. Katiyar, A. Parui, R. Das, R. Kumar, C. S. Tiwary, A. K. Singh, A. Halder and K. Biswas, *Nano Res.*, 2022, **15**, 4799-4806.

S3. J. Tang, J. L. Xu, Z. G. Ye, X. B. Li and J. M. Luo, *Journal of Materials Science & Technology*, 2021, **79**, 171-177.

S4. J. X. Yang, B.-H. Dai, C.-Y. Chiang, I. C. Chiu, C.-W. Pao, S.-Y. Lu, I. Y. Tsao, S.-T. Lin, C.-T. Chiu, J.-W. Yeh, P.-C. Chang and W.-H. Hung, *Acs Nano*, 2021, **15**, 12324-12333.

S5. F. Liu, M. Yu, X. Chen, J. Li, H. Liu and F. Cheng, *Chin. J. Catal.*, 2022, **43**, 122-129.

S6. H. Wang, R. Wei, X. Li, X. Ma, X. Hao and G. Guan, *Journal of Materials Science & Technology*, 2021, **68**, 191-198.

S7. Y. X. Sun, Q. G. Cai, Z. Wang, Z. C. Li, Q. Y. Zhou, X. Li, D. Y. Zhao, J. F. Lu, S. Q. Tian, Y. Li and S. F. Wang, *ACS Appl. Mater. Interfaces*, 2024, **16**, 23054-23060.

S8. K. Gu, X. Zhu, D. Wang, N. Zhang, G. Huang, W. Li, P. Long, J. Tian, Y. Zou, Y. Wang, R. Chen and S. Wang, *J. Energy Chem.*, 2021, **60**, 121-126.

S9. K. Huang, B. Zhang, J. Wu, T. Zhang, D. Peng, X. Cao, Z. Zhang, Z. Li and Y. Huang, *J. Mater. Chem. A*, 2020, **8**, 11938-11947.

S10. Y. Mei, Y. Feng, C. Zhang, Y. Zhang, Q. Qi and J. Hu, *ACS Catal.*, 2022, **12**, 10808-10817.

S11. W. Dai, X. Yang, F. Hu, W. Cao, C. Zhao, Y. Zhang and S. Huang, *J. Alloy. Compd.*, 2023, **952**, 169987.

S12. W. H. Antink, S. Lee, H. S. Lee, H. Shin, T. Y. Yoo, W. Ko, J. Shim, G. Na, Y.-E. Sung and T. Hyeon, *Adv. Funct. Mater.*, 2024, **34**, 2309438.

S13. T. X. Nguyen, Y. C. Liao, C. C. Lin, Y. H. Su and J. M. Ting, *Adv. Funct. Mater.*, 2021, **31**, 2101632.

S14. T. X. Nguyen, Y. H. Su, C. C. Lin, J. Ruan and J. M. Ting, *Adv. Sci.*, 2021, **8**, 2002446.

S15. J. Zhang, T. Quast, W. He, S. Dieckhoefer, J. R. C. Junqueira, D. Oehl, P. Wilde, D. Jambrec, Y.-T. Chen and W. Schuhmann, *Adv. Mater.*, 2022, **34**, 2109108.

S16. Y. Zhang, W. Dai, P. Zhang, T. Lu and Y. Pan, *J. Alloy. Compd.*, 2021, **868**, 159064.

S17. Z. Sun, Y. Zhao, C. Sun, Q. Ni, C. Wang and H. Jin, *Chem. Eng. J.*, 2022, **431**, 133448.

S18. L. He, H. Kang, G. Hou, X. Qiao, X. Jia, W. Qin and X. Wu, *Chem. Eng. J.*, 2023, **460**, 141675.

S19. P. Li, X. Wan, J. Su, W. Liu, Y. Guo, H. Yin and D. Wang, *ACS Catal.*, 2022, **12**, 11667-11674.

S20. W. Luo, Y. Wang, L. Luo, S. Gong, M. Wei, Y. Li, X. Gan, Y. Zhao, Z. Zhu and Z. Li, *ACS Catal.*, 2022, **12**, 1167-1179.

S21. A. Karmakar, T. G. Senthamaraikannan, E. Baasanjav, P. Bandyopadhyay, B. Jin, Y. S. Park, D.-H. Lim and S. M. Jeong, *Appl. Catal. B-Environ. Energy*, 2023, **328**, 122504.